12A.3 WARM SEASON RAINFALL AS A FUNCTION OF LONGITUDE AND TIME OF DAY OVER THE U.S.

D. A. Ahijevych[1], R. E. Carbone, J. D. Tuttle
National Center for Atmospheric Research[2]

1. INTRODUCTION

Following the procedure outlined in Carbone et al. (2001), the authors use 15 min. national composites of radar reflectivity to estimate meridionally-averaged rainfall rates across the U.S. for warm season months (June-August). The rainfall rates are plotted with respect to longitude and UTC time to elucidate the phase-locked zonal evolution of precipitation over a typical diurnal cycle. Salient features of this distribution include a sun-following maximum centered on 16 LST and an eastward-propagating rainfall rate maximum initiating at (105° W, 21 UTC).

This paper falls under the umbrella of a concurrent study (Carbone et al. 2001) for which meridionally-averaged seasonal time series of national radar reflectivity are used to compile seasonal statistics on the zonal span, phase speed, duration and recurrence interval of temporally and spatially coherent rainfall episodes. At the upper end of the episode spectrum are precipitation events that persist longer than 24 h or have a zonal span greater than 1250 km. Carbone et al. found that these long-lived events are not exceedingly rare; their recurrence interval is only two days. The characteristic phase speed of these events suggest that synoptic influences probably play only a minor role in their maintenance and their duration greatly exceeds the lifespan of a single mesoscale convective complex (Laing and Fritsch 1997). Inspection of two-dimensional radar time series usually reveals a chain of mesoscale convective systems (MCSs) responsible for the longer episodes (>36 h). 12- to 36-h forecasts of summertime precipitation stand to benefit from a better physical understanding of the linkage between these successive MCSs. Please refer to Carbone et al. (this preprint volume) for further information on this work, and visit http://www.mmm.ucar.edu/episodes for updates and related publications.

The strong signals in the daily averaged rainfall rate diagram illustrate the cumulative effect of many warm season rainfall episodes that regularly occur at the same time of the day or night at a particular longitude. They illustrate the heavy influence of the solar cycle and topography in the regional precipitation climatology for summer months in the U.S.

[1] NCAR, Boulder, CO, 80307-3000, ahijevyc@ucar.edu
[2] NCAR is sponsored by the National Science Foundation.

2. METHODOLOGY

This diurnal climatology of estimated rainfall rate is based on five years of data (1996-2000) covering June-August using the national mosaic of radar reflectivity produced by Weather Services International (WSI) Corporation. Using all available tilt angles, WSI merges WSR-88D radar reflectivity volumes into a two-dimensional mosaic over the U.S. with 16 5-dBZ$_e$ reflectivity levels, beginning with level 0 (0-5 dBZ$_e$). Although the exact algorithm by which WSI integrates single-site radar data into a national composite is proprietary information, it is generally understood that the mosaic contains the highest reflectivity found within the vertical column centered above each grid point. The reflectivity data is mapped to a cylindrical equidistant projection with 1837 rows and 3661 columns, and a grid spacing of approximately 2 km. Known as the NOWrad^{TM} Master Sector, this product is produced every 15 minutes, and is subject to three levels of quality control, including manual filtering of bad data.

Our domain of interest is 30°-48° N and 115°-78° W (see Fig. 1 in Carbone et al., this preprint volume). For this study, the domain was divided into north-south strips of width 0.2° and the average rainfall rate within each strip was calculated for each 15-min. interval in the 24-h day.

We applied a standard power-law transformation to the radar reflectivity (Z; mm^{6}m^{-3}) to achieve rain rate (R; mmh^{-1}):

$$Z = 300\ R^{1.4}$$

This transformation renders a relatively small net bias in the global average when compared to national analyses of rainfall (Klazura et al., 1999).

Many high-reflectivity radar artifacts were removed at WSI. However, some high-reflectivity pixels (unrelated to precipitation) made it into our database and threatened to contaminate the precipitation estimates. Therefore, we treat meridionally-averaged rainfall rates above 4.2 mmh^{-1} as missing data. This threshold effectively eliminates most high rainfall rate outliers while retaining valid rainfall rate estimates.

3. CUMULATIVE DAILY RAINFALL

There are many uncertainties in deriving rainfall from radar reflectivity. One must assume an equilibrium drop size distribution (DSD) and then compute an appropriate Z-R relationship. Considering the great natural variability of DSDs within a precipitation system, from storm to storm, and from region to region (Brandes

et al. 1999), the choice of a single representative Z-R relationship is somewhat dubious. Not surprisingly, potential Z-R relationships abound in the literature (Wilson and Brandes 1979). Uncertainty is also introduced by the 5-dBZ$_e$ quantization of radar reflectivity in the NOWrad^{TM} product (a 5 dBZ$_e$ increase is proportional to more than a factor of 2 increase in estimated rainfall rate). In addition, the lack of radar coverage over Canada and the Atlantic Ocean reduce the meridionally-averaged rainfall rate estimates in the east. Therefore, the rainfall rate is divided by the fractional radar coverage at each longitude (within the domain of interest and assuming a 200 km effective range from each WSR-88D radar). Fig. 1 shows the 24-h rainfall estimates before and after this correction.

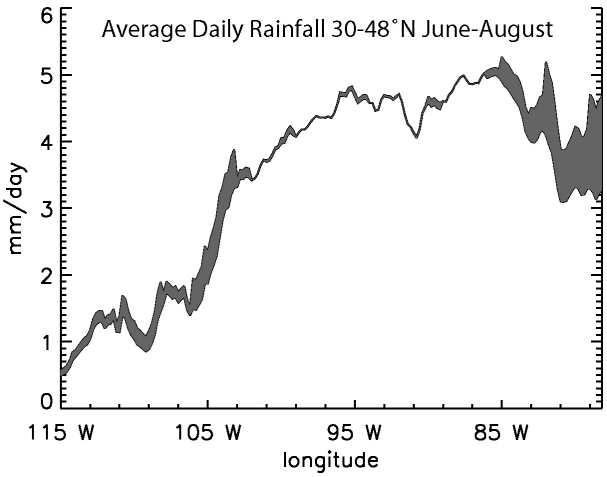

Fig. 1. Average daily rainfall in mm day^{-1} between 30° and 48° N from 1 June through 31 August. A simple correction factor was applied to the data to account for points within the domain where surface rainfall estimates would tend to be low (>200 km from any radar). The shaded area corresponds to this correction. It is largest east of 85° W where the domain overlaps Canada and the Atlantic Ocean. No attempt is made to correct for beam blockage.

Despite the uncertainties inherent in utilizing a single Z-R relationship, the radar-derived rainfall rate estimates are comparable to estimates derived from rain gauges (within a factor of 2). Figs. 1 and 2 show the 24-h rainfall as calculated from the rainfall rate integrated over 24 hours. Also shown in Fig. 2 are meridionally-averaged daily rainfall estimates from Legates and Willmott (1990) and the Global Precipitation Climatology Centre (GPCC; 1999). Over land, the Legates and Willmott global climatology of mean monthly precipitation relies entirely on gauge measurements, as do the estimates from GPCC; they are independent of radar data. Compared to the rain gauge estimates, the radar estimates are biased high. However, the general trend of low rainfall in the west with a rapid increase from 105° W to 95° W, and a leveling off further east is represented.

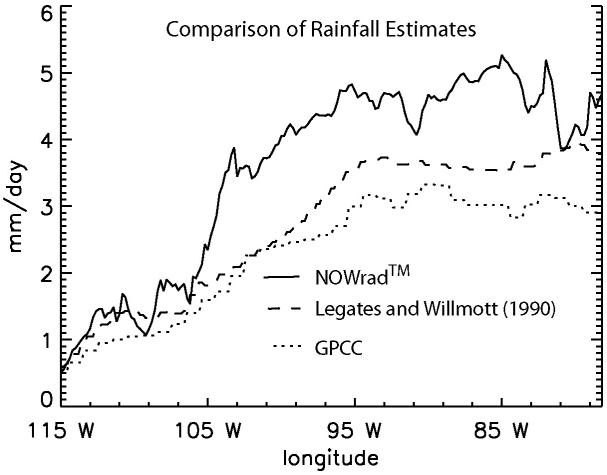

Fig. 2. Corrected daily rainfall as in Fig. 1 along with corresponding meridional averages from Legates and Willmott (1990) and GPCC. These are both based on surface rain gauge measurements. The GPCC data is based on three available years (1996-1998). The radar-derived rainfall is biased high relative to the rain gauge data, but the general trends are comparable.

4. RESULTS

Maximum average rainfall rates occur in the afternoon between 13 and 18 LST (18 and 01 UTC) over the eastern U.S. The rapid onset of high rain rates and their gradual decline probably reflects the combined effects of sudden thunderstorm development and the slow transition to more steady stratiform precipitation in decaying orphan anvils or the stratiform region of mature MCSs. The afternoon rainfall maximum is notably weaker between 101° W and 93° W, while amplifying once again in the lee of the Rockies and westward.

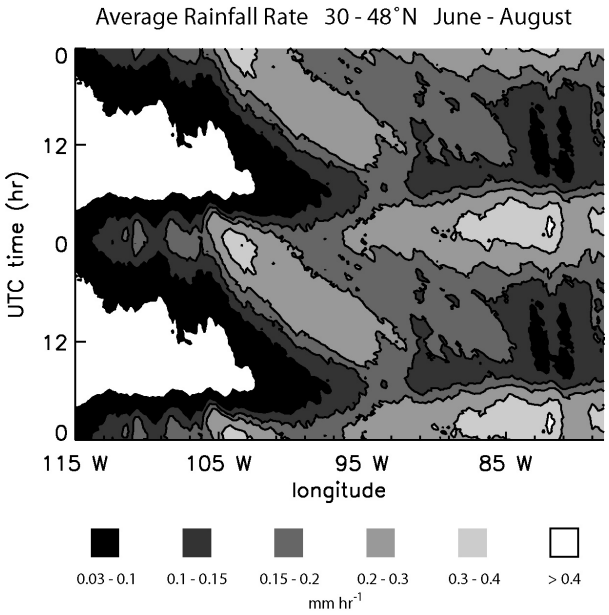

Fig. 3. Average rainfall rate between 30° and 48° N from 1 June through 31 August as a function of longitude and UTC time (hr). The data is repeated along the UTC time dimension. Note the sun-following maximum centered on 16 LST and an eastward-propagating rainfall rate maximum initiating at (105° W, 21 UTC).

This out-of-phase relation between the diurnal precipitation cycle over elevated terrain of the Rocky Mountains and the Great Plains region has been noted in the past. Wallace (1975) studied hourly surface observations of precipitation and found a similar pattern. He noted that in the lee of the Rockies, the greatest chance of precipitation is around 1800 LST (~01 UTC); as one moves eastward, there is a gradual transition to a nocturnal maximum over the high plains and finally to a 0600 LST (~12 UTC) maximum in the low plains. Processes capable of producing the boundary layer convergence necessary for this nocturnal maximum include a uniform heating cycle over sloping terrain (Holton, 1966; Lettau, 1967) and the low-level jet (Blackadar, 1957; Bonner, 1968).

Repeated thunderstorm initiation in the lee of the Rockies within a limited time window (23-00 UTC) is responsible for the narrowly bounded maximum at (105°W, 23 UTC). Virtually no precipitation is recorded during other times of the day. Subsequently, the maximum shifts eastward with a phase speed between 11 and 32 m s^{-1} (the average slopes of the 0.15 mm hr^{-1} contour). The range of phase speeds leads to an increasingly diffuse precipitation track in the seasonal average. It is difficult to track the feature beyond (93°W, 12 UTC), even though Carbone et al. (2001) showed that it is likely many of the individual events extend into the second or third diurnal cycle and to the eastern edge of the domain.

ACKNOWLEDGEMENTS

This research was sponsored by National Science Foundation support to the U.S. Weather Research Program. The authors wish to thank the Distributed Active Archive Center (Code 902) at Goddard Space Flight Center, Greenbelt, MD, 20771, for producing rainfall data in its present format and distributing them. The original data products were produced by the science investigator Dr. Bruno Rudolf at GPCC, Deutscher Wetterdienst, Germany. Goddard's share in these activities was sponsored by NASA's Mission to Planet Earth program. The authors are also deeply appreciative for assistance received from the National Climatic Data Center, the website of NOAA/CIRES Climate Diagnostics Center at U. of Colorado, S. Goodman of NASA's Marshall Spaceflight Center, NOAA/CIRA at Colorado State University, NOAA/NESDIS, and our sister organizations at NCAR/UCAR, namely the Research Applications Program and COMET. These organizations provided access to datasets critical to the analyses.

REFERENCES

Blackadar, A. K., 1957: Boundary layer wind maxima and their significance for the growth of nocturnal inversions. *Bull. Amer. Meteor. Soc.*, **38**, 283-290.

Brandes, E. A., J. Vivekanandan and J. W. Wilson: A comparison of radar reflectivity estimates of rainfall from collocated radars. *J. Atmos. Oceanic Technol.*, **16**, 1264-1272.

Carbone et al., 2001: *J. Atmos. Sci.* (submitted).

Global Precipitation Climatology Centre. (1999, June 22). Climatology Interdisciplinary Data Collection: Global rain gauge analysis from GPCC. Retrieved March 2001, from the World Wide Web: http://daac.gsfc.nasa.gov/CAMPAIGN_DOCS/FTP_SITE/INT_DIS/readmes/gpcc.html

Klazura, G. E., et al., 1999: *J. Atmos. Oceanic Technol.*, **16**, 1842-1850.

Laing, A. G. and J. M. Fritsch, 1997: The global population of mesoscale convective complexes. *Quart. J. Roy. Meteor. Soc.*, **123,** 389-405.

Legates, D. R. and C. J. Willmott: Mean seasonal and spatial variability in gauge-corrected, global precipitation. *J. Climatol.*, **10**, 111-127.

Wallace, J. M., 1975: Diurnal variations in precipitation and thunderstorm frequency over the conterminous United States. *Mon. Wea. Rev.*, **103**, 406-419.

Wilson, J. W. and E. A. Brandes: Radar measurement of rainfall, a summary. *Bull. Amer.Meteor. Soc.*, **60,** 1048-1058.